

# Bound and continuum-embedded states of cyanopolyynes anions<sup>†</sup>

Wojciech Skomorowski, Sahil Gulania, and Anna I. Krylov<sup>a</sup>

Cyanopolyynes anions were among the first anions discovered in the interstellar medium. The discovery have raised questions about routes of formation of these anions in space. Some of the proposed mechanisms assumed that anionic excited electronic states, either metastable or weakly bound, play a key role in the formation process. Verification of this hypothesis requires detailed knowledge of the electronic states of the anions. Here we investigate bound and continuum states of four cyanopolyynes anions,  $\text{CN}^-$ ,  $\text{C}_3\text{N}^-$ ,  $\text{C}_5\text{N}^-$ , and  $\text{C}_7\text{N}^-$ , by means of *ab initio* calculations. We employ the equation-of-motion coupled-cluster method augmented with complex absorbing potential. We predict that already in  $\text{CN}^-$ , the smallest anion in the family, there are several low-lying metastable states of both singlet and triplet spin symmetry. These states, identified as shape resonances, are located between 6.3–8.5 eV above the ground state of the anion (or 2.3–4.5 eV above the ground state of the parent radical) and have widths of a few tenths of eV up to 1 eV. We analyze the identified resonances in terms of leading molecular orbital contributions and Dyson orbitals. As the carbon chain length increases in the  $\text{C}_{2n+1}\text{N}^-$  series, these resonances gradually become stabilized and eventually turn into stable valence bound states. The trends in energies of the transitions leading to both resonance and bound excited states can be rationalized by means of the Hückel model. Apart from valence excited states, some of the cyanopolyyne anions can also support dipole bound states and dipole stabilized resonances, owing to a large dipole moment of the parent radicals in the lowest  $^2\Sigma^+$  state. We discuss the consequences of open-shell character of the neutral radicals on the dipole-stabilized states of the respective anions.

## 1 Introduction

Electronic spectra of typical anions are markedly different from those of neutral molecules and cations<sup>1–4</sup>. Neutral and positively charged species have numerous electronically excited bound states, particularly near the ionization threshold where an infinite series of Rydberg states appears. Yet typical anions only support a few (if any) electronically bound states<sup>5–7</sup>. Electronic states of anions can be broadly classified into the following categories: valence, dipole-bound, and correlation-bound states<sup>1,3,4,8–10</sup>. Bound excited valence states are rare due to relatively low electron detachment energy. Dipole-bound states (DBS) are reminiscent of Rydberg states in neutral systems, however, due to a different type of long-range interaction (charge – dipole instead of long-range Coulomb potential), DBS are less ubiquitous and only appear when the neutral precursor possesses sufficiently large dipole moment<sup>1,4,11–14</sup>. A separate class of electronically excited states of anions comprises auto-detaching resonances<sup>4,15</sup>, i.e., states with finite lifetime located above the lowest electron detachment threshold; those include singly excited states (which can be shape or Feshbach type) and doubly excited Feshbach resonances derived by electron attachment to an electronically excited neutral core<sup>16</sup>. Often such metastable states are the only (semi)-discrete features of anionic spectra; thus, they play an important role in their spectroscopic characterization<sup>17–19</sup>.

The discovery of simple anions in the interstellar medium (ISM) in the last decade has stimulated interest in chemical properties of these species.  $\text{C}_6\text{H}^-$ , identified in 2006<sup>20</sup>, became the

first known ISM anion. So far, five other molecular anions have been confirmed to be present in the ISM:  $\text{C}_4\text{H}^-$ ,  $\text{C}_8\text{H}^-$ ,  $\text{CN}^-$ ,  $\text{C}_3\text{N}^-$ , and  $\text{C}_5\text{N}^-$ <sup>21–25</sup>. These observations, possible routes of the formation of these anions, and theoretical modeling of their abundances are summarized in a recent review<sup>26</sup>. Astrophysical discoveries of anions in the ISM were accompanied by laboratory measurements of rotational transitions and quantum-chemical calculations, which were instrumental for the correct assignment of the observed spectra<sup>27–31</sup>. All interstellar anions identified so far are closely related and belong to the class of linear polyynes ( $\text{C}_{2n}\text{H}^-$ ) or cyanopolyyne anions ( $\text{C}_{2n-1}\text{N}^-$ ), species with the conjugated chains of triple CC and CN bonds. Their ground states have closed-shell electronic configuration ( $^1\Sigma^+$ ), giving rise to large electron detachment energy of about  $\sim 4$  eV. Several theoretical studies of (cyano)polyynes anions focused on their ground-state spectroscopic properties<sup>28,32–35</sup>. The most comprehensive study by Botschwina and Oswald<sup>28</sup> reported equilibrium structures, dipole moments, vertical detachment energies, and rotational-vibrational parameters for the  $\text{C}_{2n-1}\text{N}^-$  anions using the highly accurate CCSD(T) method (coupled-cluster with single, double and non-iterative triple excitations). In contrast to the well-studied rovibrational structure of the  $\text{C}_{2n-1}\text{N}^-$  anions<sup>28–30,32–36</sup>, their electronic spectra, in particular in the continuum part, have not been systematically investigated. Better understanding of excited states in these simple anions is important not only for the astrochemical research, but also in the context of precision spectroscopy<sup>37,38</sup> and recently proposed experiments with cold molecular anions<sup>39,40</sup> to study properties of matter at the quantum limit, where electronically excited states play a key role.

Here we characterize electronically excited bound and near-threshold continuum states of four cyanopolyynes anions  $\text{C}_{2n-1}\text{N}^-$  ( $n = 1, \dots, 4$ ) with high-level *ab initio* methods. The results are particularly relevant in the context of the ongoing discus-

<sup>a</sup> Department of Chemistry, University of Southern California, Los Angeles, California 90089, USA; E-mail: krylov@usc.edu (A.I.K.), skomorow@usc.edu (W.S.).

<sup>†</sup> Electronic Supplementary Information (ESI) available: CAP parameters,  $\eta$  trajectories, details of complex basis function and cross section calculations, relevant Cartesian geometries and basis set details.

sion on possible mechanisms of their formation in the ISM<sup>41–45</sup>. One hypothesis is that the cyanopolyynes anions might be formed via direct electron attachment to the respective neutral precursors (cyanopolyynes radicals) that are ubiquitous in the ISM, followed by spontaneous radiative transition to the anionic ground state. This radiative electron attachment (REA) process has been studied recently in the three smallest cyanopolyynes anions<sup>45</sup>; the calculations showed that the direct REA rates appear too small to explain the abundance of these anions in the ISM. The efficiency of the electron capture process can be significantly enhanced by metastable and weakly bound electronic states in the vicinity of the electron detachment threshold. These electronic states can resonantly trap incident electrons for a finite time, such that the complex can be stabilized and subsequently relax to the ground state of the anion. This mechanism can be described as indirect radiative electron attachment<sup>46</sup>. Thus, electronic or mixed electronic-vibrational resonances can act as a doorway towards efficient formation of valence bound anions by providing a mechanism for initial binding of the excess electron. A similar mechanism, electron attachment facilitated by the  $p$ -wave shape resonances, has been reported for closed-shell acetylenic carbon-rich neutral molecules (such as  $\text{NC}_4\text{N}$  and  $\text{HC}_3\text{N}$ )<sup>47–49</sup>. The prospects for the enhancement of REA via near-threshold excited anionic electronic states were discussed in Ref. 43, where it was suggested that REA may be particularly effective in strongly polar species that are likely to form near-threshold bound or metastable states.

Several theoretical studies attempted to investigate the existence of bound and metastable states in the shortest  $\text{C}_{2n-1}\text{N}^-$  anions. Harrison and Tennyson performed electron scattering calculations for  $\text{CN}+e^-$  and  $\text{C}_3\text{N}+e^-$  by using the  $R$ -matrix method<sup>50,51</sup>; this study reported several triplet resonances in  $\text{CN}^-$  (in the energy range from 3 to 5 eV above the electron detachment threshold) and singlet and triplet resonances in  $\text{C}_3\text{N}^-$  (from 0.7 to 3 eV above the threshold). Additionally, several very weakly bound  $\Sigma^+$  and  $\Pi$  states have been claimed to exist in  $\text{C}_3\text{N}^-$ . No analysis in terms of orbital character or electronic configurations has been given for aforementioned resonances and bound states<sup>50,51</sup>. The report<sup>50,51</sup> of numerous near-threshold bound states in  $\text{C}_3\text{N}^-$  contradicts the findings of previous quantum-chemical calculations<sup>13</sup> performed with EOM-CCSD method (equation-of-motion CCSD)<sup>52–54</sup> in which no bound states were found in  $\text{C}_3\text{N}^-$ . A later study<sup>55</sup> revisited these EOM-CCSD results and concluded that  $\text{C}_3\text{N}^-$  and  $\text{C}_5\text{N}^-$  support a single dipole-bound state. No similar studies have been reported for longer  $\text{C}_{2n-1}\text{N}^-$  chains.

The most relevant experimental study<sup>56</sup> of  $\text{C}_{2n-1}\text{N}^-$  is the measurement of photodetachment cross section for  $\text{CN}^-$  and  $\text{C}_3\text{N}^-$  at the wavelength of 266 nm (4.66 eV). The authors concluded that photodetachment by interstellar UV photons is the major destruction mechanism for these anions<sup>56</sup>. Earlier studies based on photoelectron spectra provided accurate electron detachment energies for  $\text{CN}^-$ <sup>57</sup>,  $\text{C}_3\text{N}^-$ , and  $\text{C}_5\text{N}^-$ <sup>58</sup>. The electronic absorption spectra have been reported for  $\text{C}_7\text{N}^-$  and longer cyanopolyynes anions in neon matrices<sup>59</sup>. The authors assigned the observed bands, progressively shifting to lower energies with the increas-

ing carbon chain length, to the  $^1\Sigma^+ \leftarrow X^1\Sigma^+$  transition. This assignment was primarily based on the analogy to the spectra of closed-shell neutral polyacetylenes ( $\text{HC}_{2n}\text{H}$ ).

This paper reports the calculations of the electronically excited bound and metastable states in cyanopolyynes anions  $\text{C}_{2n-1}\text{N}^-$  ( $n = 1, \dots, 4$ ). We employed the EOM-CCSD method<sup>52–54</sup> augmented by complex absorbing potential (CAP) to capture metastable states<sup>60</sup>. EOM-CCSD has shown robust performance in calculations of excited states of different nature in closed-shell and open-shell species<sup>52–54,61,62</sup>. Recent implementation of the complex-valued CAP-EOM-CCSD variant<sup>63–67</sup> extended this method to electronic resonances. We find that  $\text{C}_{2n-1}\text{N}^-$  possess a distinct series of low-lying discrete excited states of singlet and triplet spin symmetry, all classifiable as valence states. These states appear already in  $\text{CN}^-$  as resonances, i.e., above the lowest electron detachment threshold, and then become gradually stabilized, such that they turn into the bound states as the length of the carbon chain increases. Energies of the transitions that correspond to  $\pi \rightarrow \pi^*$  excitations can be rationalized within the Hückel model, which predicts lowering of the excited states in the molecules with the increasing number of  $\pi$ -conjugated bonds. Thus, the simple Hückel model retains its semi-quantitative validity even for excited states of resonance character. We analyze all identified excited states in terms of their lifetime (for the continuum part of the spectrum), orbital excitation character, Dyson orbitals, and transition dipole moments for optically bright states. The large dipole moment of the lowest  $^2\Sigma^+$  state in some of cyanopolyynes radicals suggest that they should also support dipole stabilized states. Indeed, we show that  $\text{C}_3\text{N}^-$  has dipole bound states while longer anions exhibit states which can be classified as dipole-stabilized resonances<sup>68</sup>. Finally, we discuss how the above features of electronic structure can manifest themselves in experimental observables such as cross sections for photodetachment (from anions) or electron scattering (from neutrals) and comment on the implications of our results regarding the mechanism of cyanopolyynes anions formation in the ISM.

## 2 Theoretical methods and computational details

We investigate the electronically excited states of the first four cyanopolyynes anions,  $\text{C}_{2n-1}\text{N}^-$ , both below and above the electronic continuum onset, by means of the EOM-CCSD method<sup>52–54,69</sup>. In all calculations, the reference wave function corresponds to the closed-shell ground-state CCSD solution for the respective anion with  $N$  electrons. We compute excitation energies by the EOM-EE variant of the method in which  $N$ -electron target states are described by particle-conserving excitation operators. To describe  $N$ -electron metastable states embedded in the electron-detachment continuum, we augment the standard EOM Hamiltonian by complex absorbing potential (CAP-EOM-EE-CCSD)<sup>63–65</sup>. We determine electron-detachment thresholds and properties of the parent neutral radicals by using the EOM-IP variant of the method in which target  $N - 1$ -electron states are described by EOM operators that remove one electron (i.e., 1 hole and 2-holes-one-particle). Fig. 1 illustrates target-states manifolds accessed by EOM-EE and EOM-IP.

Given our focus on metastable auto-ionizing states, we would

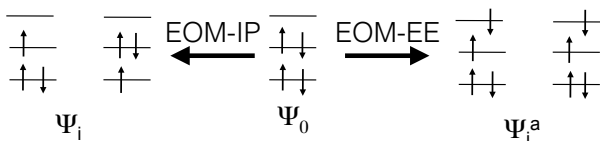


**Fig. 1** Manifolds of target states accessed by EOM-IP and EOM-EE. Here,  $\Psi_0$  denotes closed-shell CCSD wave function of the ground-state anions. The two groups of target states are described by diagonalizing the same model Hamiltonian  $\hat{H}$  obtained by the similarity transformation using the reference CCSD amplitudes.

like to highlight the advantages of the EOM-CCSD approach for treating resonances<sup>60</sup>. EOM-CC is a robust theoretical framework capable of treating diverse types of electronic structure. The method yields size-intensive transition energies (excitation, ionization, attachment) and their accuracy can be systematically improved towards the exact solution. In the context of metastable and near-threshold bound states, one of the major advantages of the EOM-CC approach is that it provides a balanced description of different target states as a result of employing the same model Hamiltonian in different EOM variants. Hence, the onsets of the continua in the EOM-EE calculations correspond exactly to the electron detachment energies obtained in the EOM-IP calculations. Consequently, energy differences are consistent with each other and one can unambiguously distinguish between the bound and continuum states.

Use of CAP allows one to represent metastable states with  $\mathcal{L}^2$ -integrable basis functions<sup>70–72</sup>. In the CAP calculations, regular Hamiltonian  $\hat{H}_0$  is augmented by an imaginary potential  $-i\eta\hat{W}$ :

$$\hat{H}(\eta) = \hat{H}_0 - i\eta\hat{W}(r) \quad (1)$$

where  $\eta$  is the strength of the CAP. This purely imaginary potential absorbs the diverging tail of the continuum states and transforms them into  $\mathcal{L}^2$ -integrable wave functions with complex energies<sup>73</sup>, which can be computed by standard *ab initio* approaches designed for bound states<sup>63,64,66,74–76</sup>. The CAP technique is related to exterior complex scaling method<sup>77</sup>. In the present study, we use the CAP-EOM-CCSD implementation reported in Refs. 63–65. Our calculations closely follow the protocol presented in those papers. The CAP is introduced as a quadratic potential of a cuboid shape:

$$\begin{aligned} \hat{W}(r) &= \hat{W}_x(r_x) + \hat{W}_y(r_y) + \hat{W}_z(r_z), \\ \hat{W}_\alpha(r) &= \begin{cases} 0 & \text{if } |r_\alpha| < r_\alpha^0 \\ (|r_\alpha| - r_\alpha^0)^2 & \text{if } |r_\alpha| > r_\alpha^0, \end{cases} \end{aligned} \quad (2)$$

where the coordinates  $(r_x^0, r_y^0, r_z^0)$  define the onset of CAP in each direction. Following the same strategy as in previous calculations<sup>63,64</sup>, we fixed the CAP onset at spatial extent of the wave function for the reference state,  $r_i^0 = \sqrt{\langle \Psi_{CCSD} | R_i^2 | \Psi_{CCSD} \rangle}$ , where  $\Psi_{CCSD}$  is the CCSD solution (CAP-free) for the ground state of the anion<sup>78</sup>. The CAP-augmented Hamiltonian yields complex eigenvalues  $E(\eta) = E_R(\eta) - i\Gamma(\eta)/2$  where  $E_R$  is the position of the resonance and  $\Gamma(\eta)$  is its width. The optimal value of the CAP

strength parameter  $\eta$  is determined for each metastable state by calculating  $\eta$ -trajectories and searching for the minimum of the function<sup>70</sup>:

$$|\eta \cdot \frac{dE(\eta)}{d\eta}| = \min, \quad (3)$$

which minimizes the error introduced by the incompleteness of the one-electron basis set and finite strength of CAP. In some cases, more robust and stable resonance parameters can be obtained if, instead of considering the raw trajectories  $E(\eta)$ , one analyzes the  $\eta$ -trajectories of deperturbed energies ( $U(\eta)$ ) from which the explicit dependence on CAP is removed in the first order<sup>64,65</sup>. The deperturbed complex energies  $U(\eta)$  are calculated by subtracting from raw energies  $E(\eta)$  the correction  $i\eta \text{Tr}[\gamma W]$  where  $\gamma$  is the one-particle density matrix of the resonance state.

Characters of the excited states can be illuminated by Dyson orbitals and transition dipole moments<sup>79</sup>. We also used EOM-CC Dyson orbitals to compute the photoelectron dipole matrix element needed for calculating of photodetachment cross section from anionic species. In these calculations the outgoing electron was represented by plane waves, similarly to our previous studies<sup>80</sup>.

Unless otherwise specified, in excited-state calculations we employ the aug-cc-pVTZ basis set<sup>81</sup> augmented with an extra set of diffuse function (mostly  $3s3p$ ) centered on each atom. The exponents of these additional functions were obtained in the same way as in our previous studies<sup>63–65</sup>. The calculations were performed at the fixed equilibrium geometries of the respective anions. The optimal geometries of the anions were taken from the literature. They correspond either to the experimental values ( $\text{CN}^-$ )<sup>57</sup> or highly accurate theoretical optimization at the CCSD(T)/aug-cc-pVQZ level [ $(\text{C}_3\text{N}^-)$ <sup>35</sup>,  $(\text{C}_5\text{N}^-)$ <sup>28</sup>,  $(\text{C}_7\text{N}^-)$ <sup>28</sup>]. The Cartesian coordinates are given in the Supplementary Information. In calculations of the adiabatic detachment energies, we optimized the structures of the neutral precursors by EOM-IP-CCSD/cc-pVTZ. The electronic structure calculations reported here were performed using the Q-Chem package<sup>82,83</sup>.

### 3 Results

All cyanopolyyne anions considered in this work are linear species with alternating single and triple bonds (Fig. 2). In the ground state, they have a closed-shell electronic configuration of  $1\Sigma^+$  symmetry. The molecular orbital analysis of the detached and excited states studied here reveals that two classes of orbitals are involved in the relevant electronic transitions. The first class com-

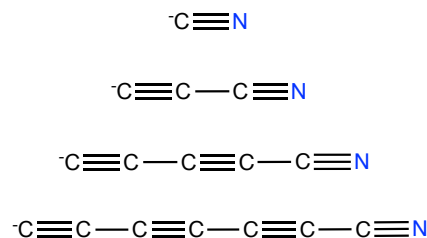


**Fig. 2** Four cyanopolyyne anions studied in this work.

prises the two sets of orthogonal and degenerate  $\pi$  orbitals. The second class comprises lone pair located on the terminal carbon

**Table 1** Vertical detachment energies (VDE) of the anions (in eV) and dipole moments  $\mu$  (in debye) of the neutral radicals.

Molecule	VDE ( ${}^2\Sigma^+$ )	$\mu$ ( ${}^2\Sigma^+$ )	VDE ( ${}^2\Pi$ )	$\mu$ ( ${}^2\Pi$ )
CN $^-$	3.99	1.35	5.28	0.18
C $_3$ N $^-$	4.67	3.87	4.79	0.14
C $_5$ N $^-$	4.98	5.86	4.70	0.11
C $_7$ N $^-$	5.22	7.97	4.71	0.03

— this orbital is of a  $\sigma$  type. The  $\pi$  system in the C $_{2n-1}$ N $^-$  anions is similar to the  $\pi$  system in conjugated polyynes. Hence, one can employ the Hückel model to interpret the trend in energies of the  $\pi$  orbitals with respect to the carbon chain length. In accordance with the Hückel model predictions, the energy of the frontier  $\pi$  orbitals increases (as does the respective detachment energy) and the energy of  $\pi^*$  orbitals decreases, as the length of the carbon chain increases. This trend is illustrated in Fig. 3. In contrast, the  $\sigma$  orbital becomes more bound in longer carbon chains, which can be rationalized in terms of electrostatic interaction between the lone electron pair and the increasing dipole moment of the neutral core.

The opposite trends in energetics of the frontier occupied orbitals ( $\pi$  and  $\sigma$ ) clearly manifest themselves in the computed electron detachment energies. Table 1 presents calculated vertical detachment energies for the two lowest detached states of  ${}^2\Sigma^+$  and  ${}^2\Pi$  symmetry. A  ${}^2\Sigma^+$  radical is obtained by removing an electron from the  $\sigma$  orbital of the anion, whereas electron detachment from  $\pi$  orbital leads to a  ${}^2\Pi$  radical, as illustrated by the shapes of the corresponding Dyson orbitals in Fig. 4.

As expected, the Dyson orbitals for the  ${}^2\Sigma^+$  states have axial symmetry with highest electron density at the carbon end of the chain. The Dyson orbitals for the  ${}^2\Pi$  states have a typical nodal structure of  $\pi$  orbitals and are delocalized over the entire chain, following the Hückel model prediction (Fig. 3). Table 1 shows that all anions have large electron detachment energy:  $\sim 4$  eV or more. Forming  ${}^2\Sigma^+$  radicals is more favorable in shorter carbon chains, whereas  ${}^2\Pi$  radicals become preferable in longer species, which leads to the change of the ground state from  ${}^2\Sigma^+$  to  ${}^2\Pi$  as

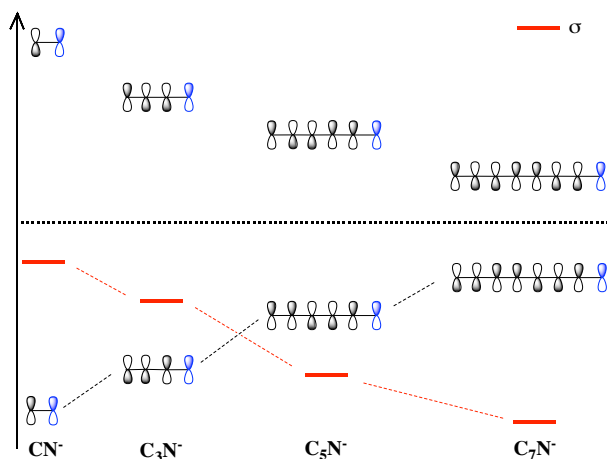


**Fig. 3** Frontier molecular orbitals in cyanopolyynes anions.

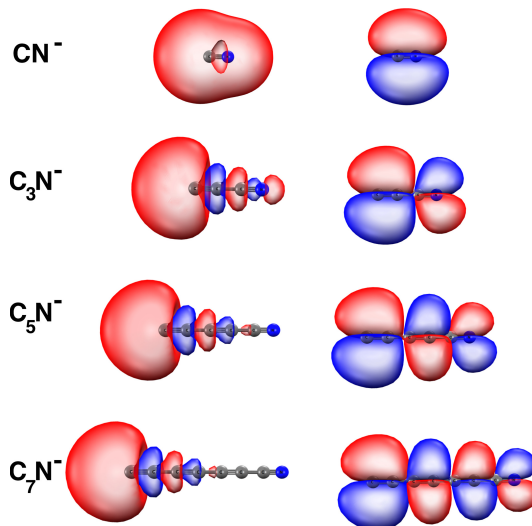


**Fig. 4** Dyson orbitals of cyanopolyynes anions corresponding to formation of the  ${}^2\Sigma^+$  (left) or  ${}^2\Pi$  (right) neutral radicals.

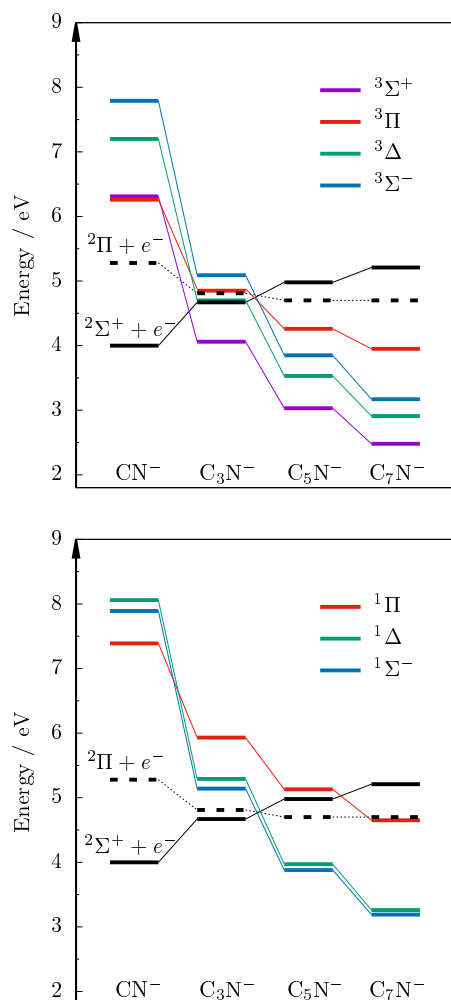


**Fig. 5** Valence excited states in cyanopolyynes anions. Top panel: triplet states, bottom panel: singlet states. Black lines mark the two lowest electron detachment thresholds corresponding to formation of  ${}^2\Sigma^+$  (solid) or  ${}^2\Pi$  (dashed) neutral radicals.

the carbon chain increases. Directly comparable with experimental measurements are adiabatic detachment energies (ADE). Table 2 summarizes our calculated ADEs together with the available experimental values<sup>57,58,84</sup>. The discrepancies between the theory and experiment are within 0.2–0.3 eV, as expected for EOM-CCSD. According to our calculations, the cross-over between the  $^2\Sigma^+$  and  $^2\Pi$  states occurs in  $C_5N$ , both adiabatically and vertically. The most recent photoelectron spectroscopic study<sup>58</sup> found that the ground state of  $C_5N$  is still  $^2\Sigma^+$ , whereas the  $^2\Pi$  state is located  $0.069 \pm 0.015$  eV above the  $^2\Sigma^+$  threshold. Thus, a higher level of electron correlation treatment beyond EOM-CCSD is necessary to exactly reproduce the cross-over between these two nearly degenerate states of  $C_5N$ .

An important property of the  $C_{2n-1}N$  radicals is their dipole moment, which is given in Table 1 for the two lowest electronic states. The states of  $^2\Sigma^+$  symmetry have large dipole moment, which increases with the length of the carbon chain. The  $^2\Pi$  states behave differently – their dipole moment remains small, independently of the molecular size. These trends in the dipole moments have two consequences. First, it explains the stabilization of the lone pair orbital, as seen in the energies of the  $^2\Sigma^+$  detached states. Second, it means that the neutral  $C_{2n-1}N$  radicals should be capable of forming dipole-bound states<sup>1,11</sup> (or dipole-stabilized resonances<sup>68</sup>) only if they are in the  $^2\Sigma^+$  state, but not in the  $^2\Pi$  state (in other words, dipole-stabilized states should correspond to the excitation of an electron from the  $\sigma$  orbital to a diffuse target orbital near the carbon end).

The electron detachment energies determine the thresholds that separate bound and unbound (metastable) excited states. The valence excited states of cyanopolyynes anions studied in the present work are predominantly the excitations from the frontier  $\sigma$  or  $\pi$  orbital into the unoccupied  $\pi^*$  orbital. The  $\sigma \rightarrow \pi^*$  transition may result in singlet or triplet  $\Pi$  states, whereas the  $\pi \rightarrow \pi^*$  transition can give rise to singlet or triplet  $\Sigma^+$ ,  $\Sigma^-$ , or  $\Delta$  states. Several possible excited states symmetries result from double degeneracy of  $\pi$ -system. Fig. 5 shows energies of all low-lying valence excited states, either metastable or bound. These energy diagrams illustrate that all excited states of  $\sigma \rightarrow \pi^*$  and  $\pi \rightarrow \pi^*$  character become stabilized with the increasing length of the carbon chain. The rate of stabilization is different in the excited states derived from the  $\pi \rightarrow \pi^*$  transitions and in those derived by the  $\sigma \rightarrow \pi^*$  excitations. The trend in the energies of all  $\pi \rightarrow \pi^*$  transitions can be rationalized in terms of the Hückel model. The

**Table 2** Adiabatic detachment energies (in eV). Theoretical values neglect zero point energy contributions.

Molecule	$^2\Sigma^+$	$^2\Pi$
CN <sup>-</sup> (this work)	3.99	5.16
Exp. (Ref. 57)	$3.862 \pm 0.004$	
C <sub>3</sub> N <sup>-</sup> (this work)	4.54	4.75
Exp. (Ref. 58)	$4.305 \pm 0.001$	
Exp. (Ref. 84)	$4.59 \pm 0.25$	
C <sub>5</sub> N <sup>-</sup> (this work)	4.79	4.69
Exp. (Ref. 58)	$4.45 \pm 0.03$	

$\sigma \rightarrow \pi^*$  transitions follow a different pattern, determined by the opposing trends in the  $\pi^*$  and  $\sigma$  orbitals. More thorough analysis of these trends in electronic spectra is given in Section 3.4, after detailed results for each species, starting from CN<sup>-</sup>, the prototype of all cyanopolyynes anions.

### 3.1 CN<sup>-</sup>

CN<sup>-</sup> is the precursor of the cyanopolyynes series. Owing to its small size, it often serves as a benchmark system amenable to high-level quantum-chemical calculations. CN<sup>-</sup> and its parent radical CN play important roles not only in the ISM and astrochemistry, but also in combustion chemistry, carbon-rich plasmas, rotational spectroscopy, and in precision measurements of cosmological properties<sup>30,85,86</sup>. Our CAP-EOM-EE-CCSD calculations identified seven valence low-lying resonances of different symmetries. Their positions and linewidths are reported in Table 3 and the  $\eta$  trajectories used to extract the resonance parameters are given in the Supplementary Information. The energies are given with respect to the ground state of CN<sup>-</sup>. The resonances are located in the range of 6.3 to 8.5 eV above the ground state, that is, more than 2 eV above the lowest CN<sup>-</sup> detachment threshold. They are all predominantly  $\pi \rightarrow \pi^*$  excitations, except for the  $^1\Pi$  and  $^3\Pi$  states that correspond to  $\sigma \rightarrow \pi^*$  transition.

All states can decay to a parent radical ( $^2\Sigma^+$  or  $^2\Pi$ ) in one-electron process, thus, they can be classified as shape resonances. Inspection of Table 3 shows that all singlet resonances are slightly broader than the triplets of the same symmetry and that they are higher in energy. The results obtained from the uncorrected trajectories ( $E_R^{(0)}$ ,  $\Gamma^{(0)}$ ) and the first-order corrected trajectories ( $E_R^{(1)}$ ,  $\Gamma^{(1)}$ ) differ by no more than 0.1 eV for the position of the resonances and by no more than 0.25 eV for the widths. The optimal velocities, Eq. (3), obtained from the first-order corrected trajectories  $v^{(1)}$  are systematically lower than those from the uncorrected trajectories  $v^{(0)}$ , confirming that the correction<sup>64</sup> indeed improves the accuracy of the resonance determination. The small size of cyanide allows us to test the convergence of the results with respect to the size of the one-electron basis set. This is summarized in Table 4, which presents the positions and widths of the CN<sup>-</sup> resonances obtained with three different basis sets. Table 4 shows that the smallest tested basis set (aug-cc-pVTZ+3s3p) gives already satisfactory results for the resonance parameters, in particular, for the narrowest resonances. In most cases, larger valence or more diffuse basis sets lead to slightly lower resonance positions and smaller widths. Importantly, in all cases, the resonance parameters obtained with our basic basis set (aug-cc-pVTZ+3s3p) are reasonably close to the position and widths obtained with larger basis sets. On the basis of these benchmarks, for larger cyanopolyynes anions we employ only the aug-cc-pVTZ+3s3p basis set.

To further validate our results from CAP calculations, we computed the resonance parameters for the CN<sup>-</sup> triplet states with the complex basis function (CBF) method<sup>87,88</sup> (see Supplementary Information for the details). The results from the CAP (Table 4) and from the CBF (Table SII) calculations compare favorably, reaffirming our predictions of resonance states in CN<sup>-</sup>. We

**Table 3** Positions  $E_R$ , widths  $\Gamma$  (eV), optimal values of  $\eta$  parameter, and corresponding trajectory velocities (in atomic units) for low-lying resonances in  $\text{CN}^-$ . Basis set is aug-cc-pVTZ+3s3p. Numbers in parentheses denote powers of 10.

State	$E_R^{(0)}$	$\Gamma^{(0)}$	$\eta_{\text{opt}}^{(0)}$	$\nu^{(0)}$	$E_R^{(1)}$	$\Gamma^{(1)}$	$\eta_{\text{opt}}^{(1)}$	$\nu^{(1)}$
$^3\Sigma^+(\pi \rightarrow \pi^*)$	6.34	0.20	0.0034	1.2(-3)	6.31	0.16	0.007	5.9(-4)
$^3\Pi(\sigma \rightarrow \pi^*)$	6.62	0.61	0.055	4.5(-3)	6.56	0.45	0.12	3.0(-3)
$^3\Delta(\pi \rightarrow \pi^*)$	7.51	0.58	0.055	4.7(-3)	7.45	0.42	0.10	2.1(-3)
$^3\Sigma^-(\pi \rightarrow \pi^*)$	8.18	0.64	0.055	4.4(-3)	8.19	0.48	0.12	2.1(-3)
$^1\Pi(\sigma \rightarrow \pi^*)$	7.90	0.79	0.064	3.7(-3)	7.88	0.56	0.18	2.0(-3)
$^1\Delta(\pi \rightarrow \pi^*)$	8.54	0.70	0.056	4.5(-3)	8.49	0.52	0.14	1.5(-3)
$^1\Sigma^-(\pi \rightarrow \pi^*)$	8.29	0.65	0.052	4.4(-3)	8.23	0.48	0.12	2.0(-3)

can also directly compare our results for  $\text{CN}^-$  with the  $R$ -matrix calculations of Harrison and Tennyson<sup>51</sup>. They reported three triplet resonances ( $^3\Sigma^+$ ,  $^3\Pi$  and  $^3\Sigma^-$ ), located 3.2 to 4.9 eV above the lowest electron detachment threshold with widths around  $\sim 1$  eV (see Table 3 in Ref. 51 for the exact numbers obtained with different electronic structure models employed within the  $R$ -matrix approach). Due to strong dependence of the  $R$ -matrix results on the electronic structure model, the authors estimated the uncertainty in their reported widths up to 50%. When compared with our results, it appears that the method applied in Ref. 51 yields larger resonance widths, which led to the conclusion that singlet resonances are not supported by  $\text{CN}^-$ . Several other studies computed excited states in  $\text{CN}^-$  using methods for bound electronic states<sup>89–91</sup>. Interestingly, potential energy curves for  $\text{CN}^-$  from Ref. 90 show that  $^3\Sigma^+$  state becomes stable with respect to electron detachment at the bond length beyond  $\sim 2.9$  bohr. This prediction is in line with our CAP results showing that the  $^3\Sigma^+$  resonance is the most narrow one at the equilibrium structure. Another reason why the  $^3\Sigma^+$  state is potentially the most easily stabilized resonance is that it is the only state that asymptotically correlates with the lowest atomic threshold:  $\text{C}^- (^4S_u) + \text{N} (^4S_u)$ . This threshold is located about 1.26 eV below the lowest  $\text{C} (^3P_g) + \text{N} (^4S_u)$  asymptote, meaning that sufficiently stretched  $\text{CN}^-$  must have stable (with respect to electron detachment) excited states of  $^3\Sigma^+$ ,  $^5\Sigma^+$ , and  $^7\Sigma^+$  symmetry.

We can also relate our results for metastable states of  $\text{CN}^-$  to the electronic structure of isoelectronic diatomic molecules,  $\text{NO}^+$  (Ref. 92) and  $\text{N}_2$  (Ref. 93). All predicted  $\text{CN}^-$  resonances follow closely the pattern of the low-lying excited states in  $\text{NO}^+$  and  $\text{N}_2$ .

**Table 4** Positions  $E_R$  (and widths  $\Gamma$ ), in eV, of the resonances in  $\text{CN}^-$  calculated with various basis sets.

	aug-cc-pVTZ +3s3p	aug-cc-pVQZ +3s3p	aug-cc-pVTZ +4s4p3d
$^3\Sigma^+$	6.34 (0.20)	6.35 (0.19)	6.31 (0.19)
$^3\Pi$	6.62 (0.61)	6.49 (0.49)	6.26 (0.51)
$^3\Delta$	7.51 (0.58)	7.40 (0.45)	7.20 (0.38)
$^3\Sigma^-$	8.18 (0.64)	8.03 (0.52)	7.79 (0.55)
$^1\Pi$	7.90 (0.79)	7.69 (0.74)	7.39 (1.05)
$^1\Delta$	8.54 (0.70)	8.37 (0.57)	8.06 (0.70)
$^1\Sigma^-$	8.29 (0.65)	8.15 (0.52)	7.89 (0.58)

For example,  $\text{NO}^+$  possesses a manifold of valence excited states in the energy range of 6.3 – 9.0 eV above the ground state, which have exactly the same symmetries and orbital characters as the computed  $\text{CN}^-$  resonances. Similarly to  $\text{CN}^-$ , neither  $\text{NO}^+$  nor  $\text{N}_2$  have low-lying excited states of the  $^1\Sigma^+$  symmetry that can be derived from the  $\pi \rightarrow \pi^*$  transition.

### 3.2 $\text{C}_3\text{N}^-$

Results of the CAP-EOM-CCSD calculations for  $\text{C}_3\text{N}^-$ , the second cyanopolyne anion, are presented in Table 5. The low-lying resonances of  $\text{C}_3\text{N}^-$  appear at lower energies relative to  $\text{CN}^-$ . The  $^3\Sigma^+$  state is below the lowest detachment threshold and, therefore, is bound with respect to electron detachment. While being red-shifted, all  $\text{C}_3\text{N}^-$  resonances also become more narrow by roughly one order of magnitude relative to  $\text{CN}^-$ . Table 5 shows that the observed stabilization effect is accompanied by much lower optimal values of the CAP strength parameter  $\eta$  and much lower corresponding trajectory velocities. This means that determination of resonances parameters for  $\text{C}_3\text{N}^-$  should be more robust and less basis set dependent than for  $\text{CN}^-$ . While the  $^3\Sigma^+$  state became a valence bound state, the  $^3\Delta$  state changed its character from shape to Feshbach resonance, i.e., the  $^3\Delta$  state (of  $\sigma^2\pi^2\pi\pi^*$  electronic configuration) is located below its parent neutral state of the  $\text{C}_3\text{N}$  radical ( $^2\Pi$ , electron configuration  $\sigma^2\pi^2\pi$ ) but can still autoionize producing the  $^2\Sigma$  state of  $\text{C}_3\text{N}$  (of  $\sigma\pi^2\pi^2$  electronic configuration) via two-electron transition. This change in the resonance character leads to longer lifetime and ultra-narrow resonance width, lower than the accuracy of our method. This is why for the  $^3\Delta$  resonance we were only able to obtain an upper bound of the width.

Similarly to  $\text{CN}^-$ , the metastable electronic states of  $\text{C}_3\text{N}^-$  were investigated by the  $R$ -matrix method<sup>50</sup>. Comparison of our results with those given in Table 7 of Ref. 50 shows qualitative similarity between the CAP-EOM-EE-CCSD and  $R$ -matrix resonance parameters. In both calculations, the order of all resonance states is the same and the  $\text{C}_3\text{N}^-$  resonances are significantly more narrow than the corresponding states in  $\text{CN}^-$ . The most notable difference is in the widths, which are a few times larger in the  $R$ -matrix calculations. Moreover, the resonances in the  $R$ -matrix calculations appear about 1.5 eV higher than in the CAP-EOM-CCSD calculations. Slightly different geometries employed in the two studies would not account for the discrepancies

**Table 5** Positions  $E_R$ , widths  $\Gamma$  (in eV), optimal values of  $\eta$  parameter, and corresponding trajectory velocities (in atomic units) for low-lying resonances in  $C_3N^-$ .  ${}^3\Sigma^+$  is a bound state. Basis set is aug-cc-pVTZ+3s3p. Numbers in parentheses denote powers of 10.

State	$E_R^{(0)}$	$\Gamma^{(0)}$	$\eta_{\text{opt}}^{(0)}$	$\nu^{(0)}$	$E_R^{(1)}$	$\Gamma^{(1)}$	$\eta_{\text{opt}}^{(1)}$	$\nu^{(1)}$
${}^3\Sigma^+(\pi \rightarrow \pi^*)$	4.06	—						
${}^3\Pi(\sigma \rightarrow \pi^*)$	4.85	0.015	0.00065	1.2(-4)	4.85	0.011	0.0016	5.0(-5)
${}^3\Delta(\pi \rightarrow \pi^*)$	4.68	< 0.001			4.68			
${}^3\Sigma^-(\pi \rightarrow \pi^*)$	5.10	0.017	0.0010	1.4(-4)	5.10	0.012	0.0018	8.7(-5)
${}^1\Pi(\sigma \rightarrow \pi^*)$	5.94	0.152	0.0085	6.6(-4)	5.92	0.123	0.0150	1.5(-4)
${}^1\Delta(\pi \rightarrow \pi^*)$	5.30	0.029	0.0010	1.7(-4)	5.29	0.025	0.0020	1.8(-4)
${}^1\Sigma^-(\pi \rightarrow \pi^*)$	5.16	0.022	0.0015	1.7(-4)	5.16	0.017	0.0030	1.5(-4)

in resonance predictions; rather, those discrepancies arise due to the differences in the description of the continuum and its coupling to the bound part of the spectrum as well as approximations in the many-body treatment. In principle, the hermitian R-matrix scattering approach is well suited for treating resonances. However, the many-body nature of the molecular electronic problem implies that other factors, i.e., electron correlation treatment and one-electron basis sets, contribute to the observed discrepancies. This is confirmed by significant discrepancies across different electronic structure models employed in the R-matrix study, as can be seen in Table 7 of Ref. 50. A systematic comparison of the two approaches (CAP-EOM-CCSD and R-matrix) would be very meaningful in this context.

### 3.3 $C_5N^-$ and $C_7N^-$

Table 6 contains the results of the CAP-EOM-CCSD and EOM-CCSD calculations for the two longest cyanopolyne anions considered in the present work:  $C_5N^-$  and  $C_7N^-$ . In  $C_5N^-$ , only the  ${}^1\Pi$  state remains a resonance, with a very small width of less than 0.02 eV. Other valence excited states drop below the lowest detachment threshold and become stable with respect to autoionization. The recent theoretical study of the  $C_5N^-$  photodetachment<sup>45</sup> reported the sharp  ${}^1\Pi$  shape resonance at 5.1 eV, which agrees well with our calculations. Fortenberry in his EOM-CCSD calculations for  $C_5N^-$  reported a valence bound  ${}^1\Sigma^+$  excited state at around 4.0 eV<sup>55</sup>. Our results suggest that this is actually  ${}^1\Delta$  excited state. Our symmetry assignment is consistent with an extremely small oscillator strength ( $\sim 10^{-6}$ ) for the transition to the anion ground state reported in Ref. 55.

In  $C_7N^-$  the lowest-lying  $\pi \rightarrow \pi^*$  and  $\sigma \rightarrow \pi^*$  transitions are stabilized even further, such that even the  ${}^1\Pi$  state becomes bound. Thus,  $C_7N^-$  anion supports seven bound excited states, which is quite remarkable for an anion. What is not shown in Table 6 and Fig. 5 is a new low-lying resonance of  ${}^1\Sigma^+$  symmetry emerging in  $C_7N^-$ . This new state of a mixed valence-diffuse character is discussed below, in Sec. 3.5 devoted to dipole-stabilized states. We note that  $C_7N^-$  has additional low-lying valence resonances approaching the electron detachment threshold corresponding to excitations from deeper  $\pi$  occupied orbitals. They are located about 2 eV above the lowest valence states of the same symmetry, which are reported in Table 6. Here we do not discuss these states, since our focus is on the lowest transitions, i.e., originating

from the highest occupied  $\pi$  or  $\sigma$  orbitals.

**Table 6** Excitation energies (eV) of low-lying valence states of  $C_5N^-$  and  $C_7N^-$ . Basis set is aug-cc-pVTZ+3s3p.

State	$C_5N^-$	$C_7N^-$
${}^3\Sigma^+(\pi \rightarrow \pi^*)$	3.03	2.48
${}^3\Pi(\sigma \rightarrow \pi^*)$	4.26	3.94
${}^3\Delta(\pi \rightarrow \pi^*)$	3.52	2.90
${}^3\Sigma^-(\pi \rightarrow \pi^*)$	3.85	3.17
${}^1\Pi(\sigma \rightarrow \pi^*)$	5.12 <sup>a</sup>	4.69
${}^1\Delta(\pi \rightarrow \pi^*)$	3.98	3.26
${}^1\Sigma^-(\pi \rightarrow \pi^*)$	3.88	3.19

<sup>a</sup>This state is a resonance with the following parameters:  $E_R^{(0)} = 5.12$  eV,  $\Gamma^{(0)} = 0.017$  eV,  $\nu^{(0)} = 1.1 \times 10^{-4}$ ,  $E_R^{(1)} = 5.13$  eV,  $\Gamma^{(1)} = 0.016$  eV,  $\eta_{\text{opt}}^{(1)} = 2.4 \times 10^{-3}$ ,  $\nu^{(1)} = 1.9 \times 10^{-5}$ .

### 3.4 General trends in electronic spectra

It is instructive to assemble and compare the results for all cyanopolyne anions studied in the present work. Figure 5 shows that the energies of all  $\pi \rightarrow \pi^*$  transitions decrease to a similar extent as the carbon chain lengths increases. As mentioned above, this can be rationalized in terms of the Hückel model description of  $\pi$ -conjugated systems. According to the Hückel's model, in a  $\pi$  system comprised of  $N$  atoms in a linear chain, the lowest  $\pi \rightarrow \pi^*$  (HOMO-LUMO) transition energy reads:

$$e_{\text{LUMO}} - e_{\text{HOMO}} = -4\beta \sin \frac{\pi}{2(1+N)},$$

and it depends only on one parameter  $\beta$ . We determined optimal  $\beta$  values for each of the  $\pi \rightarrow \pi^*$  excitations by least squares fitting. Figure 6 compares *ab initio* transition energies with those from the Hückel model based on fitted  $\beta$ 's for each of the transitions. The optimal  $\beta$  values vary between  $-3.25$  and  $-4.33$  eV. The variation in  $\beta$  values is not surprising, as we describe multiple states of different spin and spatial symmetry with the same model. Similarly, different  $\beta$ 's are used to describe singlet/triplet transitions in conjugated hydrocarbon molecules<sup>94</sup>. In all cases shown in Fig. 6 there is a reasonably good agreement, highlighting the regularity in the excitation energies in the cyanopolyne anions. Remarkably, the Hückel model is capable of reproducing consistently the transitions to both metastable and bound states.

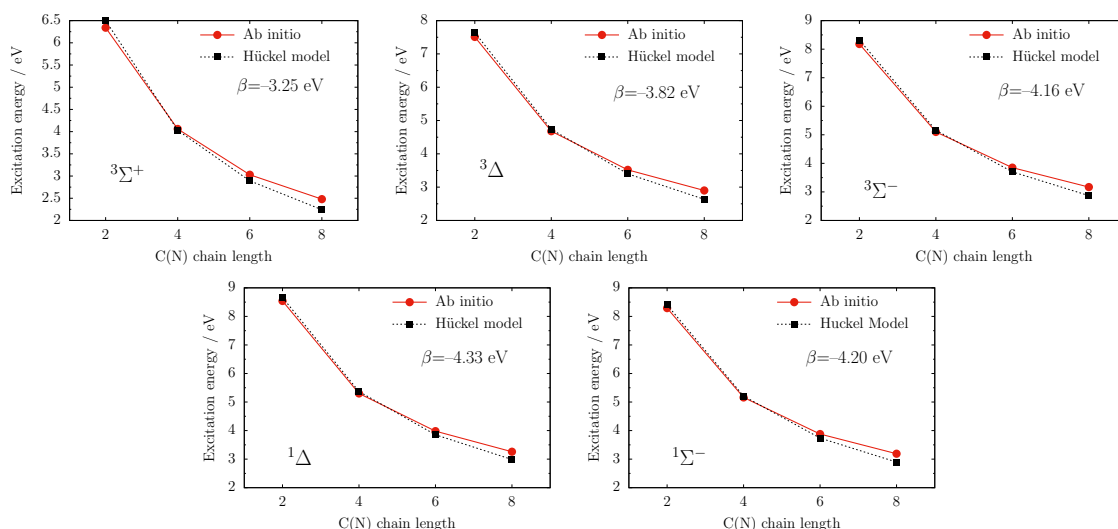


**Fig. 6** Excitation energies of  $\pi\pi^*$  states from *ab initio* calculations and from the Hückel model.

The agreement between the two curves in Fig. 6 can be made almost perfect if one allows for slightly different values of the resonance integrals  $\beta$  for CN and CC bonds.

The energies of metastable states are lowered and their widths become more and more narrow with the increasing chain length. This behavior is explained by increased delocalization, which is captured by the Huckel model. In addition, polarization, which increases in longer carbon chains, may also contribute towards resonance stabilization<sup>95,96</sup>. Consequently, metastable states undergo gradual stabilization in longer species and eventually become bound. This trend is also illustrated in Fig. 5 when the excited states shift down and drop below the lowest neutral threshold (marked with black solid or dashed lines in Fig. 5). As mentioned above, all  $\text{CN}^-$  resonances are of shape type because they can autoionize via a one-electron transition. This is true for all resonances located above both ( ${}^2\Sigma$  and  ${}^2\Pi$ ) neutral thresholds. If a metastable state drops below its parent neutral but is still above the other neutral threshold, then it becomes a Feshbach resonance. We observe such situation only for the  ${}^3\Delta$  state: it is a shape resonance in  $\text{CN}^-$ , Feshbach resonance in  $\text{C}_3\text{N}^-$ , and, finally, a stable bound state in  $\text{C}_5\text{N}^-$  and  $\text{C}_7\text{N}^-$ . All other metastable states are converted directly from shape resonances into stable bound states.

Comparing widths of the singlet and triplet resonances of the same symmetry, we note that, in all cases, the singlet states are broader than triplets. A possible reason is that the singlet continuum has a higher density of states than the triplet continuum due to Pauli exclusion principle excluding some of the electronic configurations of the same-spin electrons. Consequently, the coupling of singlet metastable states with the continuum is stronger and their lifetimes are shorter.

A common feature of all valence resonances and bound states shown in Fig. 5 is that they are dominated by one-electron excitation into the lowest unoccupied  $\pi^*$  orbital. This is best illustrated by the Dyson orbitals of the excited states calculated as overlaps with the corresponding parent radical ( ${}^2\Pi$  neutral for  ${}^3\Sigma^+$ ,

${}^{1/3}\Sigma^-$  and  ${}^{1/3}\Delta$ , or  ${}^2\Sigma^+$  neutral for  ${}^{1/3}\Pi$  excited states). Figure 7 shows illustrative Dyson orbitals for the identified  ${}^1\Pi$  states (either metastable or bound). Both real and imaginary parts of all Dyson orbitals have typical nodal structure of  $\pi^*$  orbitals. Their norms<sup>97</sup> are almost purely real and equal to  $\sim 0.47 - 0.002i$  ( $\Pi$  states) and  $0.24 + 0.003i$  ( $\Sigma^+$ ,  $\Sigma^-$  and  $\Delta$  states). Relatively small norms of the Dyson orbitals indicate importance of correlation.

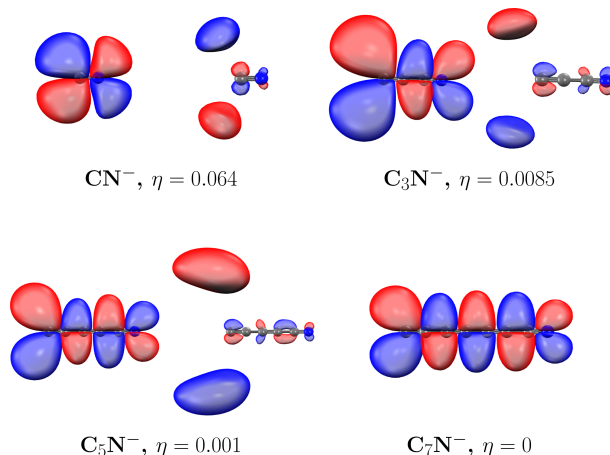


**Fig. 7** Real (left-hand side in each panel) and imaginary (right-hand side in each panel) parts of Dyson orbitals for the  ${}^1\Pi$  state in cyanopolyne anions. Dyson orbitals were calculated as the overlap with the lowest  ${}^2\Sigma^+$  state of the corresponding parent radical.

Of all the identified valence resonances, the  ${}^1\Pi$  state is the most interesting, as it is directly accessible via one-photon transition from the  ${}^1\Sigma^+$  ground state of the anion. This state can be observed in one-photon photodetachment (or absorption cross) section. Also, it can serve as a gateway in a two-step radiative electron attachment, a process discussed in the context of possible mechanisms of  $\text{C}_{2n-1}\text{N}^-$  formation in the ISM.

### 3.5 In the search of dipole-stabilized states in cyanopolyynes

The discussion above focused exclusively on valence excited states. Let us now discuss states derived by excitation into diffuse orbitals and stabilized by the electrostatic interaction between the outer electron and the dipole moment of the neutral core. These can be either dipole-bound states or dipole-stabilized resonances. According to the results in Table 1,  $C_3N^-$  is most likely to support dipole bound states because its parent radical in the electronic ground state has dipole moment exceeding the critical value<sup>98</sup> of  $\sim 2.5$  D. In longer anions, DBS would require excitation from a lower-lying  $\sigma$  orbital. To locate DBS, we carried out EOM-EE-CCSD calculations<sup>99</sup> with extended basis sets which included up to  $8s$ ,  $5p$  and  $1d$  additional diffuse functions on top of the aug-cc-pVTZ basis set. In  $C_3N^-$  we found two weakly bound states ( $^3\Sigma^+$  and  $^1\Sigma^+$ ), located just below the lowest electron detachment threshold. Our best estimates of the vertical binding energies (computed at the equilibrium structure of the anion) are 0.006 eV for the  $^3\Sigma^+$  state and 0.002 eV for the  $^1\Sigma^+$  state, obtained with the aug-cc-pVTZ+8s5p1d basis set. Interestingly, although the parent radical  $C_3N$  has considerably large dipole moment ( $\sim 3.9$  D), the binding energies of the DBS states are extremely small. For example, these binding energies are 2-6 times smaller than in DBS in closely related  $HC_3N^-$ , which has closed-shell precursor with  $\mu=4.2$  D. We attribute these weak stabilization energies to the open-shell character of the parent radical. Detailed discussion of this issue will be presented elsewhere. In contrast to the previous EOM-CCSD studies<sup>13,55</sup> in which the excitation energies of putative DBS states never dropped below the detachment threshold, in our calculations the identification of DBS as bound states is unambiguous. We did not find DBS in other cyanopolyynes ( $CN^-$ ,  $C_5N^-$  and  $C_7N^-$ ), which is consistent with low values of dipole moments of the respective neutral precursors in their electronic ground states. However, the CAP-augmented EOM-CCSD calculations for  $C_5N^-$  and  $C_7N^-$  identified low-lying excited states of  $\Sigma^+$  symmetry, which can be described as dipole-stabilized resonances. These states, dominated by the excitation from frontier  $\sigma$  into diffuse  $\sigma^*$  orbital, appear between 5.1 and 5.8 eV above the anionic ground state and have relatively large widths spanning from  $\sim 0.3$  to  $\sim 0.8$  eV (see Table 7 for states denoted as  $2^1\Sigma^+$  and  $2^3\Sigma^+$ ). The dipole-stabilized character of these states is revealed by the shapes of Dyson orbitals (calculated as the overlap with the

$2^3\Sigma^+$  state of parent radicals). As shown in Fig. 8a-c, the excess electron resides outside the terminal carbon, i.e., at the positive end of the dipole. The  $2^1\Sigma^+$  state of  $C_7N$  is an exception in this series, as it has a mixed  $\pi \rightarrow \pi^*$  and  $\sigma \rightarrow \sigma^*$  character. This mixing is reflected by relatively large c-norm values of Dyson orbitals computed for the two different detachment channels corresponding to the  $^2\Pi$  (c-norm is  $0.20 - 0.02i$ , Fig. 8d) and  $^2\Sigma^+$  (c-norm is  $0.08 + 0.04i$ , Fig. 8c) states of the radical. For other states, there is only one Dyson orbital with non-negligible c-norm. Significant  $\pi \rightarrow \pi^*$  character of the  $2^1\Sigma^+$  state in  $C_7N$  suggests its classification as a valence state. Therefore, this resonance is the first appearance of  $^1\Sigma^+$  excitation from the  $\pi \rightarrow \pi^*$  manifold, which was missing in shorter cyanopolyne chains (see Fig. 5).

The shapes of  $\eta$ -trajectories for the resonances of  $\sigma \rightarrow \sigma^*$  character differ considerably from those for valence-type states ( $\eta$ -trajectories for all metastable states are given in Supplementary Information). The  $\eta$ -trajectories for  $\Sigma^+$  dipole-stabilized resonances are more difficult to interpret as they feature quasi-oscillatory behavior with several stabilization points. Optimal  $\eta_{opt}$  values reported in Table 7 correspond to the lowest  $\eta$  at which stabilization is manifested both by the minimum of the trajectory velocity, Eq. (3), and by constant size of the wave function, defined as  $\langle R^2 \rangle$ .

Because the dipole moment of the CN radical is small (1.35 D), it is unlikely that this molecule would support dipole-stabilized anionic states. Quite surprisingly, the CAP-augmented EOM-CCSD calculations yield some low-lying diffuse metastable states (around 5.7 eV), derived by the excitation from  $\sigma$  orbital into diffuse  $\sigma$ -like orbitals. These states persists in CAP-EOM-CCSD calculations with larger basis sets and different CAP onsets. Similar states appear in some CBF calculations (e.g., with aug-cc-pVTZ+3s3p basis set), but they all disappear when larger basis set (aug-cc-pVTZ+6s6p or aug-cc-pVTZ+9s9p) is employed in CBF EOM-CCSD. We concluded that these states are false resonances appearing as artifacts of the theoretical approaches.

### 3.6 Possible experimental observation of the predicted features

There have been yet no experimental observation of the electronic resonances in cyanopolyne anions. Below we discuss how our predictions regarding electronic structure of  $C_nN^-$  can be verified experimentally. The easiest to observe would be the low-lying  $^1\Pi$

**Table 7** Dipole-stabilized and diffuse states of  $\Sigma^+$  symmetry in cyanopolyne anions. Metastable states (in  $C_5N^-$ ,  $C_7N^-$ ) are characterized by position  $E_R$ , width  $\Gamma$  (in eV), optimal value of  $\eta$  parameter, and corresponding trajectory velocity (in atomic units). For DBS ( $C_3N^-$ ) we report binding energy. Basis sets are: aug-cc-pVTZ+8s5p1d ( $C_3N^-$ ) and aug-cc-pVDZ+3s3p ( $C_5N^-$  and  $C_7N^-$ ). Numbers in parentheses denote powers of 10.

Anion	State	$E_R^{(0)}$	$\Gamma^{(0)}$	$\eta_{opt}^{(0)}$	$v^{(0)}$	$E_R^{(1)}$	$\Gamma^{(1)}$	$\eta_{opt}^{(1)}$	$v^{(1)}$
$C_3N^-$	$2^3\Sigma^+(\sigma \rightarrow \sigma^*)$	-0.006 <sup>a</sup>	—	—	—	—	—	—	—
	$2^1\Sigma^+(\sigma \rightarrow \sigma^*)$	-0.002 <sup>a</sup>	—	—	—	—	—	—	—
$C_5N^-$	$2^3\Sigma^+(\sigma \rightarrow \sigma^*)$	5.63	0.78	0.02	6.6(-3)	5.54	0.53	0.04	9.5(-4)
	$2^1\Sigma^+(\sigma \rightarrow \sigma^*)$	5.76	0.76	0.018	6.4(-3)	5.64	0.56	0.034	2.3(-3)
$C_7N^-$	$2^3\Sigma^+(\sigma \rightarrow \sigma^*)$	5.16	0.34	0.001	3.5(-3)	5.12	0.26	0.002	1.3(-3)
	$2^1\Sigma^+(\pi \rightarrow \pi^*)$	5.33	0.13	0.03	1.3(-3)	5.30	0.14	0.03	1.4(-3)

<sup>a</sup>Binding energy (in eV) with respect to the lowest ionization threshold.

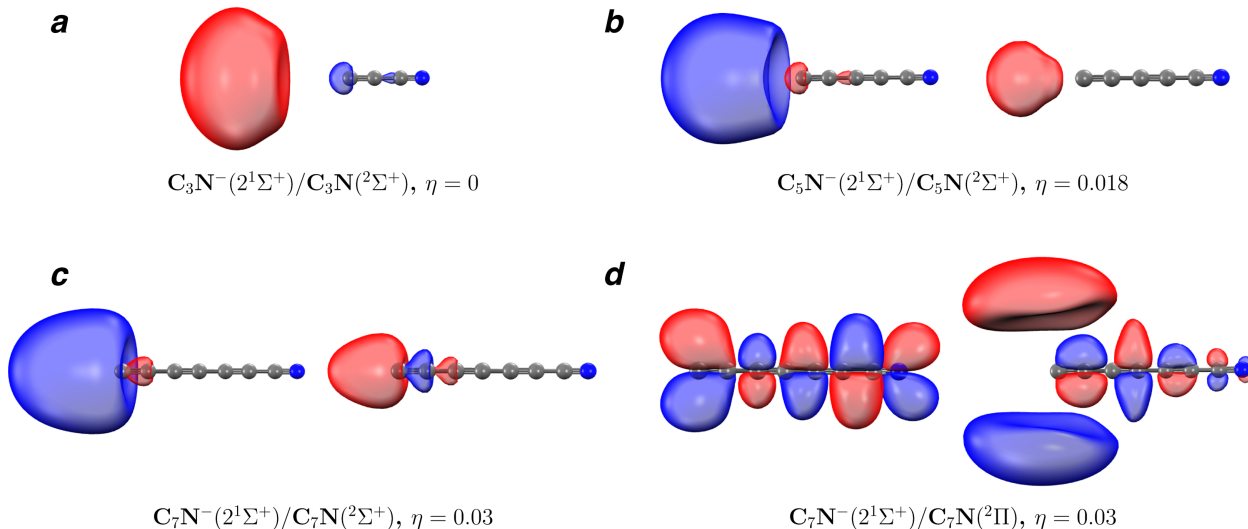


**Fig. 8** Real (left-hand side in each panel) and imaginary (right-hand side in each panel) parts of Dyson orbitals for diffuse  $^1\Sigma^+$  states reported in Table 7. Dyson orbitals were calculated as the overlap with the  $^2\Sigma^+$  state (panels a–c) or the  $^2\Pi$  state (panel d) of the corresponding parent radical.

and  $^1\Sigma^+$  resonances, as they are dipole-coupled with the anionic  $^1\Sigma^+$  ground state and should, therefore, be visible in photodetachment cross section. The calculated photodetachment cross sections are shown in Fig. 9, including the contribution due to the  $^1\Pi$  and  $^1\Sigma^+$  resonances. Details of photodetachment cross section computations are given in the Supplementary Information. The predicted resonance peaks due to the  $^1\Pi$  resonance in  $C_3N^-$  and  $C_5N^-$  are rather prominent and should be easily detected if the photodetachment cross section is measured in the appropriate energy range. Similar resonance features in the photodetachment cross section of  $C_3N^-$  and  $C_5N^-$  have been predicted in Ref. 45. For  $CN^-$  the large widths of the  $^1\Pi$  resonance makes its contribution to the total photodetachment cross section less pronounced and most of the features in the total cross section come from opening new detachment channels.

Whereas the  $^1\Pi$  and  $^1\Sigma^+$  resonances could be accessed directly from the electronic ground state of the  $C_{2n-1}N^-$  anions, other resonances, both singlets and triplets, could manifest themselves in electron scattering from the neutral  $C_{2n-1}N$  precursors, similarly to the resonances observed in electron impact experiments involving open-shell molecules such as NO<sup>100</sup>,  $(C_2^-)$ <sup>101</sup>, or  $C_2F_5$ <sup>102</sup> (via dissociative electron attachment process). One can expect prominent features in the total cross section for shape resonances asso-

ciated with electron being captured by the  $C_{2n-1}N$  ground state ( $^1\Pi$  and  $^3\Pi$  resonances in  $CN^-$  or  $C_3N^-$ ). Less pronounced peaks would appear for other shape resonances originating from the excited state of  $C_{2n-1}N$  radical ( $^3\Sigma^+$ ,  $^1\Delta$ ,  $^3\Delta$ ,  $^1\Sigma^-$ , or  $^3\Sigma^-$  states in  $CN^-$ ). In this case, resonances would preferably decay to its parent radical in the excited state ( $^2\Pi$  in  $CN^-$ ), thus enhancing the probability of the formation of excited state  $C_{2n-1}N$  (Ref. 103).

Bound excited states of cyanopolynes can be observed by absorption or emission spectroscopy. The first state of this kind is  $^3\Sigma^+$  in  $C_3N^-$ . While the optical transition from the  $X^1\Sigma^+$  ground state is spin-forbidden, this state is most likely responsible for the observed long-lived phosphorescence in  $C_3N^-$ , with the band origin at 3.58 eV in rare gas matrix<sup>104</sup> (our vertical excitation energy is 4.06 eV). Similar emission bands assigned to the  $X^1\Sigma^+ \leftarrow ^3\Sigma^+$  transition were measured for the neutral  $HC_5N$  and  $HC_7N$  molecules<sup>105,106</sup> with origins at 2.92 and 2.45 eV, respectively. These values compare favorably with our predictions for the  $^3\Sigma^+$  state in the isoelectronic  $C_5N^-$  and  $C_7N^-$  anions (vertical excitation energies of 3.03 and 2.48 eV). Bound excited states of  $^1\Sigma^+$  and  $^1\Pi$  symmetry can be directly probed by absorption spectroscopy. The absorption spectrum of  $C_7N^-$  embedded in neon matrices<sup>59</sup> reveals electronic transition with the origin at 4.53 eV. The authors assigned this transition as  $2^1\Sigma^+ \leftarrow X^1\Sigma^+$ , by anal-

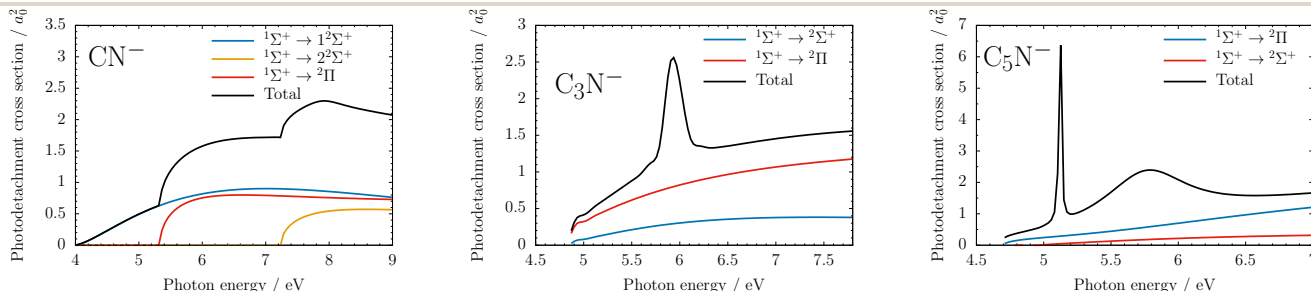


**Fig. 9** Calculated photodetachment cross sections for  $CN^-$ ,  $C_3N^-$ , and  $C_5N^-$ . Contribution from detachment to  $^2\Sigma^+$  and  $^2\Pi$  neutral states are shown separately. The sharp peaks in the total cross section are due to the  $^1\Pi$  resonance.

ogy with  $\text{HC}_{2n}\text{H}$ . Our results suggest that this feature more likely corresponds to the  ${}^1\Pi \leftarrow X{}^1\Sigma^+$  transition (vertical excitation energy of 4.69 eV, according to our calculations). However, we also predict a narrow  $2{}^1\Sigma^+$  resonance at  $\sim 5.1$  eV and lifetime of 5 fs, with large transition dipole moment to the anionic ground state (see Table SIII in the Supplementary Information). Therefore, the original assignment of the observed band as  $2{}^1\Sigma^+ \leftarrow X{}^1\Sigma^+$  cannot be ruled out, since neon matrix can stabilize the excited states and convert the resonance into a bound state. Bound excited states in anionic species can also be probed by multiphoton resonance-enhanced detachment spectroscopy, as it was demonstrated for polyatomic carbon anions<sup>107</sup>. In this technique bound excited states serve as intermediate states in multiphoton detachment. In principle, absorption spectroscopy can also detect electronic resonances if their lifetime is sufficient<sup>108</sup>. For example, the sharp  ${}^1\Pi$  resonance in  $\text{C}_5\text{N}^-$  with detachment lifetime of 40 fs can lead to discrete absorption band, despite being embedded in the continuum.

## 4 Summary and conclusions

Recent discovery of several carbon chain anions in the ISM triggered theoretical and experimental studies aiming to understand their chemical and spectroscopic properties. Such knowledge is essential to explain the molecular origin of these species in space and might also guide astrochemical search for new, yet undiscovered anions. In this contribution, we presented a systematic *ab initio* study of the electronic structure of cyanopolyne anions  $\text{C}_{2n+1}\text{N}^-$  ( $n = 0, \dots, 3$ ), with the focus on their low-lying metastable (with respect to electron detachment) and bound excited states. The calculations were carried out by the CAP-EOM-CCSD method, which describes bound and metastable states on an equal footing. Already for  $\text{CN}^-$ , the smallest anion in the series, we found several low-lying singlet and triplet metastable states ( ${}^1\Sigma^-$ ,  ${}^1\Delta$ ,  ${}^1\Pi$ ,  ${}^3\Sigma^+$ ,  ${}^3\Sigma^-$ ,  ${}^3\Delta$ ,  ${}^3\Pi$ ). These metastable states can be classified as shape resonances and correspond to valence  $\pi \rightarrow \pi^*$  or  $\sigma \rightarrow \pi^*$  excitation from the ground state of the anion. Dominant one-electron character of these states is clearly manifested in the shape of the respective Dyson orbital, which in all cases resembles a typical  $\pi^*$  orbital. In longer species, the positions of all valence metastable states are lowered and their widths decrease; eventually, these resonances become bound. The stabilization can be explained by the increased delocalization of the frontier molecular orbitals. On the route from metastable to stable bound states, some resonances might change their character from shape type to Feshbach type, as it happens for the  ${}^3\Delta$  state in  $\text{C}_3\text{N}^-$  anion. For all valence resonances, the singlets are systematically broader than the corresponding triplets of the same symmetry, indicating stronger coupling between the bound and continuum parts of the spectrum for singlet spin symmetry.

In the case of excited states of  $\pi \rightarrow \pi^*$  character (i.e.  $\Sigma^+$ ,  $\Sigma^-$  and  $\Delta$ ) trends in excitation energy as a function of carbon chain length are well reproduced by the Hückel model. Thus, the Hückel model retains its validity across the domains of bound and metastable states.

Apart from the valence metastable and bound excited states, some of cyanopolyne anions can also support dipole-stabilized

states, either bound or metastable. Their existence depends on the magnitude of dipole moment of the parent neutral radical. Our EOM-EE-CCSD calculations showed unequivocally that  $\text{C}_3\text{N}^-$  has near-threshold bound states of  ${}^1\Sigma^+$  and  ${}^3\Sigma^+$  symmetry, bound vertically by less than 0.01 eV. In longer cyanopolyne anions ( $\text{C}_5\text{N}^-$  and  $\text{C}_7\text{N}^-$ ) the CAP calculations identified relatively broad dipole-stabilized resonances.

The resonances identified in this work are located in the range from a few tenths of eV ( $\text{C}_5\text{N}^-$  and  $\text{C}_7\text{N}^-$ ) up to a few eV ( $\text{CN}^-$ ) above the ground state of the parent neutral radical. In  $\text{C}_5\text{N}^-$  the  ${}^1\Pi$  resonance appears in the energy range that might be relevant for its formation via REA, especially if we take into account the effect of structural relaxation. In the case of  $\text{C}_3\text{N}^-$  rovibrational resonances associated with the  ${}^1\Sigma^+$  DBS provide a natural doorway for the formation of the anions in the ISM via electron attachment. In this process the electron is captured into DBS Feshbach vibrational level located near the detachment threshold, and then the resulting transient state can undergo stabilization to the anion's electronic ground state via dipole-allowed transition. For the smallest interstellar anions,  $\text{CN}^-$ , the electronic structure calculations do not support mechanisms of its formation involving direct electron capture by the CN radical. We concur with the previous studies<sup>44,47,84</sup> that chemical reactions and dissociation of larger closed-shell molecules such as  $\text{NC}_3\text{N}$  or  $\text{HC}_3\text{N}$  are more likely sources of  $\text{CN}^-$  occurrence in space.

We discussed several possible ways of how the predicted resonances can manifest themselves in experimental observables, including photodetachment cross section, electron impact spectroscopy, and absorption or emission spectra (in the case of stable bound states). The easiest to observe are the  ${}^1\Pi$  and  ${}^1\Sigma^+$  states, which have non-vanishing transition dipole moment to the anion ground state; therefore, they can be probed by one-photon spectroscopy of the anion ground state.

## Conflicts of interest

A.I.K. is a member of the Board of Directors and a part-owner of Q-Chem, Inc.

## Acknowledgments

This work has been supported in Los Angeles by the Army Research Office through grant W911NF-16-1-0232 and the Alexander von Humboldt Foundation (Bessel Award to A.I.K.). We thank Dr. Thomas Jagau and Prof. Ken Jordan for stimulating discussions and feedback about the manuscript.

## References

- 1 J. Simons, *J. Phys. Chem. A*, 2008, **112**, 6401–6511.
- 2 J. Simons, *Annu. Rev. Phys. Chem.*, 2011, **62**, 107–128.
- 3 J. Simons, *Photoionization and Photodetachment*, World Scientific Publishing Co., Singapore, 2000, vol. 10, Part II.
- 4 J. M. Herbert, *Rev. Comp. Chem.*, 2015, **28**, 391–517.
- 5 W. R. Garrett, *J. Chem. Phys.*, 1982, **77**, 3666–3673.
- 6 G. L. Gutsev, M. Nooijen and R. J. Bartlett, *Chem. Phys. Lett.*, 1997, **276**, 13 – 19.
- 7 T. Sommerfeld, *Phys. Chem. Chem. Phys.*, 2002, **4**, 2511–2516.

- 8 T. Sommerfeld, B. Bhattarai, V. Vysotskiy and L. Cederbaum, *J. Chem. Phys.*, 2010, **133**, 114301.
- 9 V. K. Voora and K. D. Jordan, *J. Phys. Chem. A*, 2014, **118**, 7201–7205.
- 10 V. Voora, L. Cederbaum and K. Jordan, *J. Phys. Chem. Lett.*, 2013, **4**, 849–853.
- 11 K. Jordan and F. Wang, *Annu. Rev. Phys. Chem.*, 2003, **54**, 367–396.
- 12 M. Gutowski, K. Jordan and P. Skurski, *J. Phys. Chem. A*, 1998, **102**, 2624–2633.
- 13 R. Fortenberry and T. D. Crawford, *J. Chem. Phys.*, 2011, **134**, 154304.
- 14 K. R. Lykke, R. D. Mead and W. C. Lineberger, *Phys. Rev. Lett.*, 1984, **52**, 2221–2224.
- 15 K. Jordan, V. Voora and J. Simons, *Theor. Chem. Acc.*, 2014, **133**, 1445.
- 16 The ( $\pi\pi^*$ ) excited state of the PYP chromophore is a shape resonance in the phenolate form and a Feshbach resonance in the carboxylate form<sup>109</sup>. An example of doubly excited anionic Feshbach resonance is the  $(\pi)^{-1}(3s)^2$  state in ethylene.
- 17 K. D. Jordan and P. D. Burrow, *Acc. Chem. Res.*, 1978, **11**, 341–348.
- 18 R. Dressler and M. Allan, *J. Chem. Phys.*, 1987, **87**, 4510–4518.
- 19 J. Schiedt and R. Weinkauff, *J. Chem. Phys.*, 1999, **110**, 304.
- 20 M. C. McCarthy, C. A. Gottlieb, H. Gupta and P. Thaddeus, *Astrophys. J. Lett.*, 2006, **652**, L141.
- 21 S. Brünken, H. Gupta, C. A. Gottlieb, M. C. McCarthy and P. Thaddeus, *Astrophys. J. Lett.*, 2007, **664**, L43.
- 22 P. Thaddeus, C. A. Gottlieb, H. Gupta, S. Brünken, M. C. McCarthy, M. Agúndez, M. Guélin and J. Cernicharo, *Astrophys. J.*, 2008, **677**, 1132.
- 23 Cernicharo, J., Guélin, M., Agúndez, M., Kawaguchi, K., McCarthy, M. and Thaddeus, P., *Astronomy & Astrophysics*, 2007, **467**, L37–L40.
- 24 J. Cernicharo, M. Guélin, M. Agundez, M. C. McCarthy and P. Thaddeus, *Astrophys. J. Lett.*, 2008, **688**, L83.
- 25 M. Agúndez, J. Cernicharo, M. Guélin, C. Kahane, E. Roueff, J. Klos, F. Aoi, F. Lique, N. Marcelino, J. R. Goicoechea, M. González-García, C. Gottlieb, M. McCarthy and P. Thaddeus, *Astronomy & Astrophysics*, 2010, **517**, L2.
- 26 T. J. Millar, C. Walsh and T. A. Field, *Chem. Rev.*, 2017, **117**, 1765–1795.
- 27 H. Gupta, S. Brünken, F. Tamassia, C. A. Gottlieb, M. C. McCarthy and P. Thaddeus, *Astrophys. J. Lett.*, 2007, **655**, L57.
- 28 P. Botschwina and R. Oswald, *J. Chem. Phys.*, 2008, **129**, 044305.
- 29 M. C. McCarthy and P. Thaddeus, *J. Chem. Phys.*, 2008, **129**, 054314.
- 30 C. A. Gottlieb, S. Brünken, M. C. McCarthy and P. Thaddeus, *J. Chem. Phys.*, 2007, **126**, 191101.
- 31 K. Aoki, *Chem. Phys. Lett.*, 2000, **323**, 55 – 58.
- 32 C.-R. Wang, R.-B. Huang, Z.-Y. Liu and L.-S. Zheng, *Chem. Phys. Lett.*, 1995, **237**, 463 – 467.
- 33 C. Zhan and S. Iwata, *J. Chem. Phys.*, 1996, **104**, 9058–9064.
- 34 A. Coupeaud, M. Turowski, M. Gronowski, N. Piétri, I. Couturier-Tamburelli, R. Kołos and J.-P. Aycard, *J. Chem. Phys.*, 2008, **128**, 154303.
- 35 C. Stein, O. Weser, B. Schröder and P. Botschwina, *Mol. Phys.*, 2015, **113**, 2169–2178.
- 36 R. Kołos, M. Gronowski and P. Botschwina, *J. Chem. Phys.*, 2008, **128**, 154305.
- 37 G. Ito, T. Furukawa, H. Tanuma, J. Matsumoto, H. Shimomaru, T. Majima, M. Goto, T. Azuma and K. Hansen, *Phys. Rev. Lett.*, 2014, **112**, 183001.
- 38 G.-Z. Zhu, Y. Liu and L.-S. Wang, *Phys. Rev. Lett.*, 2017, **119**, 023002.
- 39 P. Yzombard, M. Hamamda, S. Gerber, M. Doser and D. Comparat, *Phys. Rev. Lett.*, 2015, **114**, 213001.
- 40 M. Tomza, *Phys. Chem. Chem. Phys.*, 2017, **19**, 16512–16523.
- 41 E. Herbst and Y. Osamura, *Astrophys. J.*, 2008, **679**, 1670.
- 42 F. Carelli, M. Satta, T. Grassi and F. A. Gianturco, *Astrophys. J.*, 2013, **774**, 97.
- 43 F. Carelli, F. A. Gianturco, R. Wester and M. Satta, *J. Chem. Phys.*, 2014, **141**, 054302.
- 44 M. Satta, F. A. Gianturco, F. Carelli and R. Wester, *Astrophys. J.*, 2015, **799**, 228.
- 45 M. Khamesian, N. Douguet, S. dos Santos, O. Dulieu, M. Raoult, W. Brigg and V. Kokouline, *Phys. Rev. Lett.*, 2016, **117**, 123001.
- 46 N. Douguet, S. F. dos Santos, M. Raoult, O. Dulieu, A. E. Orel and V. Kokouline, *J. Chem. Phys.*, 2015, **142**, 234309.
- 47 K. Graupner, T. A. Field and G. C. Saunders, *Astrophys. J. Lett.*, 2008, **685**, L95.
- 48 F. Sebastianelli and F. A. Gianturco, *Eur. Phys. J. D*, 2012, **66**, 41.
- 49 F. Sebastianelli and F. A. Gianturco, *Eur. Phys. J. D*, 2010, **59**, 389–398.
- 50 S. Harrison and J. Tennyson, *J. Phys. B*, 2011, **44**, 045206.
- 51 S. Harrison and J. Tennyson, *J. Phys. B*, 2012, **45**, 035204.
- 52 A. I. Krylov, *Annu. Rev. Phys. Chem.*, 2008, **59**, 433–462.
- 53 K. Sneskov and O. Christiansen, *WIREs Comput. Mol. Sci.*, 2012, **2**, 566–584.
- 54 R. Bartlett, *WIREs Comput. Mol. Sci.*, 2012, **2**, 126–138.
- 55 R. C. Fortenberry, *J. Phys. Chem. A*, 2015, **119**, 9941–9953.
- 56 S. S. Kumar, D. Hauser, R. Jindra, T. Best, S. Roucka, W. D. Geppert, T. J. Millar and R. Wester, *Astrophys. J.*, 2013, **776**, 25.
- 57 S. E. Bradforth, E. H. Kim, D. W. Arnold and D. M. Neumark, *J. Chem. Phys.*, 1993, **98**, 800–810.
- 58 T. A. Yen, E. Garand, A. T. Shreve and D. M. Neumark, *J. Phys. Chem. A*, 2010, **114**, 3215–3220.
- 59 M. Grutter, M. Wyss and J. P. Maier, *J. Chem. Phys.*, 1999, **110**, 1492–1496.
- 60 T.-C. Jagau, K. B. Bravaya and A. I. Krylov, *Annu. Rev. Phys.*

- Chem.*, 2017, **68**, 525–553.
- 61 H. Reisler and A. I. Krylov, *Int. Rev. Phys. Chem.*, 2009, **28**, 267–308.
- 62 A. I. Krylov, *Reviews in Comp. Chem.*, J. Wiley & Sons, 2017, vol. 30, ch. 4, pp. 151–224.
- 63 D. Zuev, T.-C. Jagau, K. B. Bravaya, E. Epifanovsky, Y. Shao, E. Sundstrom, M. Head-Gordon and A. I. Krylov, *J. Chem. Phys.*, 2014, **141**, 024102.
- 64 T.-C. Jagau, D. Zuev, K. B. Bravaya, E. Epifanovsky and A. I. Krylov, *J. Phys. Chem. Lett.*, 2014, **5**, 310–315.
- 65 T.-C. Jagau and A. I. Krylov, *J. Phys. Chem. Lett.*, 2014, **5**, 3078–3085.
- 66 A. Ghosh, N. Vaval and S. Pal, *J. Chem. Phys.*, 2012, **136**, 234110.
- 67 M. Ehara and T. Sommerfeld, *Chem. Phys. Lett.*, 2012, **537**, 107–112.
- 68 T.-C. Jagau, D. B. Dao, N. S. Holtgrewe, A. I. Krylov and R. Mabbs, *J. Phys. Chem. Lett.*, 2015, **6**, 2786–2793.
- 69 R. Bartlett and M. Musial, *Rev. Mod. Phys.*, 2007, **79**, 291–352.
- 70 U. V. Riss and H.-D. Meyer, *J. Phys. B*, 1993, **26**, 4503–4536.
- 71 R. Santra and L. Cederbaum, *Phys. Rep.*, 2002, **368**, 1–117.
- 72 J. Muga, J. Palao, B. Navarro and I. Egusquiza, *Phys. Rep.*, 2004, **395**, 357–426.
- 73 T. Sommerfeld and H.-D. Meyer, *J. Phys. B*, 2002, **35**, 1841–1863.
- 74 R. Santra and L. Cederbaum, *J. Chem. Phys.*, 2002, **117**, 5511–5521.
- 75 T. Sommerfeld and R. Santra, *Int. J. Quant. Chem.*, 2001, **82**, 218–226.
- 76 Y. Zhou and M. Ernzerhof, *J. Phys. Chem. Lett.*, 2012, **3**, 1916–1920.
- 77 U. Riss and H.-D. Meyer, *J. Phys. B*, 1998, **31**, 2279–2304.
- 78 Note that in EOM-EA calculations, the reference corresponds to the neutral state, whereas in EOM-EE it is the ground anionic state.
- 79 T.-C. Jagau and A. I. Krylov, *J. Chem. Phys.*, 2016, **144**, 054113.
- 80 S. Gozem, A. O. Gunina, T. Ichino, D. L. Osborn, J. F. Stanton and A. I. Krylov, *J. Phys. Chem. Lett.*, 2015, **6**, 4532–4540.
- 81 R. Kendall, J. T.H. Dunning and R. Harrison, *J. Chem. Phys.*, 1992, **96**, 6796–6806.
- 82 Shao, Y.; Gan, Z.; Epifanovsky, E.; Gilbert, A.T.B.; Wormit, M.; Kussmann, J.; Lange, A.W.; Behn, A.; Deng, J.; Feng, X., et al., *Mol. Phys.*, 2015, **113**, 184–215.
- 83 A. I. Krylov and P. M. W. Gill, *WIREs Comput. Mol. Sci.*, 2013, **3**, 317–326.
- 84 K. Graupner, T. L. Merrigan, T. A. Field, T. G. A. Youngs and P. C. Marr, *New. J. Phys.*, 2006, **8**, 117.
- 85 S. Leach, *Mon. N. Roy. Astr. Soc.*, 2012, **421**, 1325–1330.
- 86 P. Casavecchia, N. Balucani, L. Cartechini, G. Capozza, A. Bergeat and G. G. Volpi, *Faraday Discuss.*, 2002, **119**, 27–49.
- 87 A. White, M. Head-Gordon and C. McCurdy, *J. Chem. Phys.*, 2015, **142**, 054103.
- 88 A. F. White, E. Epifanovsky, C. W. McCurdy and M. Head-Gordon, *J. Chem. Phys.*, 2017, **146**, 234107.
- 89 T.-K. Ha and G. Zumofen, *Mol. Phys.*, 1980, **40**, 445–454.
- 90 R. Polák and J. Fišer, *J. Molec. Struct. (THEOCHEM)*, 2002, **584**, 69 – 77.
- 91 M. Musial, *Mol. Phys.*, 2005, **103**, 2055–2060.
- 92 H. Partridge, S. R. Langhoff and C. W. B. Jr., *J. Chem. Phys.*, 1990, **93**, 7179–7186.
- 93 W. C. Ermler, A. D. McLean and R. S. Mulliken, *J. Phys. Chem.*, 1982, **86**, 1305–1314.
- 94 I. T. R. Zahradník and J. Pancíř, *Collect. Czech. Chem. Commun.*, 1971, **36**, 2867–2880.
- 95 J. Bardsley, F. Mandl and A. Wood, *Chem. Phys. Lett.*, 1967, **1**, 359 – 362.
- 96 M. Krauss and F. H. Mies, *Phys. Rev. A*, 1970, **1**, 1592–1598.
- 97 Complex values of the norms of Dyson orbitals<sup>79</sup> are the consequence of c-norm used in non-Hermitian extensions of quantum mechanics.
- 98 O. Crawford, *Mol. Phys.*, 1971, **20**, 585–591.
- 99 We note that in order for the Davidson procedure to find these states, which have highly non-Koopmans character, it was necessary to use tighter convergence thresholds ( $10^{-6}$ ) and a much larger than usual guess space (we used 120 guess vectors).
- 100 M. Jelisavcic, R. Panajotovic and S. J. Buckman, *Phys. Rev. Lett.*, 2003, **90**, 203201.
- 101 H. B. Pedersen, N. Djurić, M. J. Jensen, D. Kella, C. P. Safvan, L. Vejby-Christensen and L. H. Andersen, *Phys. Rev. Lett.*, 1998, **81**, 5302–5305.
- 102 S. A. Haughey, T. A. Field, J. Langer, N. S. Shuman, T. M. Miller, J. F. Friedman and A. A. Viggiano, *J. Chem. Phys.*, 2012, **137**, 054310.
- 103 M. Allan, *Helv. Chim. Acta*, 1982, **65**, 2008–2023.
- 104 M. Turowski, M. Gronowski, S. Boyé-Péronne, S. Douin, L. Monéron, C. Crépin and R. Kołos, *J. Chem. Phys.*, 2008, **128**, 164304.
- 105 M. Turowski, C. Crépin, M. Gronowski, J.-C. Guillemin, A. Coupeaud, I. Couturier-Tamburelli, N. Piétri and R. Kołos, *J. Chem. Phys.*, 2010, **133**, 074310.
- 106 I. Couturier-Tamburelli, N. Piétri, C. Crépin, M. Turowski, J.-C. Guillemin and R. Kołos, *J. Chem. Phys.*, 2014, **140**, 044329.
- 107 Y. Zhao, E. de Beer, C. Xu, T. Taylor and D. M. Neumark, *J. Chem. Phys.*, 1996, **105**, 4905–4919.
- 108 M. Tulej, J. Fulara, A. Sobolewski, M. Jungen and J. P. Maier, *J. Chem. Phys.*, 2000, **112**, 3747–3753.
- 109 D. Zuev, K. B. Bravaya, T. D. Crawford, R. Lindh and A. I. Krylov, *J. Chem. Phys.*, 2011, **134**, 034310.